

## Spatial and temporal variability of surface mass balance near Talos Dome, East Antarctica

Massimo Frezzotti,<sup>1</sup> Stefano Urbini,<sup>2</sup> Marco Proposito,<sup>1</sup> Claudio Sarchilli,<sup>1,3</sup> and Stefano Gandolfi<sup>4</sup>

Received 26 July 2006; revised 21 December 2006; accepted 31 January 2007; published 13 June 2007.

[1] Predictions concerning Antarctica's contribution to sea level change have been hampered by poor knowledge of surface mass balance. Snow accumulation is the most direct climate indicator and has important implications for paleoclimatic reconstruction from ice cores. Snow accumulation measurements (stake, core, snow radar) taken along a 500-km transect crossing Talos Dome (East Antarctica) have been used to assess accumulation signals and the representativeness of ice core records. Stake readings show that accumulation hiatuses can occur at sites with accumulation rates below  $120 \text{ kg m}^{-2} \text{ yr}^{-1}$ . Differences between cores and stakes can lead to statistical misidentification of annual layers determined from seasonal signals at sites with accumulation rates below  $200 \text{ kg m}^{-2} \text{ yr}^{-1}$  because of nondetection of higher and lower values. Achieving  $\pm 10\%$  accuracy in the reconstruction of snow accumulation from single cores requires high accumulation ( $750 \text{ kg m}^{-2} \text{ yr}^{-1}$ ). Low-accumulation sites are representative if cumulative rates computed over several years are used to reach the  $750 \text{ kg m}^{-2} \text{ yr}^{-1}$  threshold. Temporal variability of accumulation over the last two centuries shows no significant increase in accumulation. Wind-driven processes are a fundamental component of surface mass balance. Spatial variations in accumulation are well correlated with surface slope changes along the wind direction and may exceed  $200 \text{ kg m}^{-2} \text{ yr}^{-1}$  within 1 km. Wind-driven sublimation rates are less than  $50 \text{ kg m}^{-2} \text{ yr}^{-1}$  in plateau areas and up to  $260 \text{ kg m}^{-2} \text{ yr}^{-1}$  in slope areas and account for 20–75% of precipitation, whereas depositional features are negligible in surface mass balance.

**Citation:** Frezzotti, M., S. Urbini, M. Proposito, C. Sarchilli, and S. Gandolfi (2007), Spatial and temporal variability of surface mass balance near Talos Dome, East Antarctica, *J. Geophys. Res.*, 112, F02032, doi:10.1029/2006JF000638.

### 1. Introduction

[2] The determination of snow accumulation rates is a major challenge in mass balance studies and in the interpretation of ice core records. Depth-age models for deep ice cores and mass balance research require knowledge of the temporal variability of snow accumulation. Snow accumulation results from precipitation in the form of snow, which is then modified by surface sublimation, erosion/deposition due to divergence/convergence of snowdrift transport, and sublimation of drifting snow particles (wind-driven sublimation). Sublimation (wind-driven and surface) removes mass from the surface, whereas erosion/deposition transports snow from one place to another.

[3] Chemical and isotopic analysis of ice cores can detect seasonal and annual signals. However, these signals may not be representative of the actual annual snow accumu-

lation value and annual snow chemical/isotopic composition. There are several sources of noise that may potentially affect snow accumulation time series [e.g., Goodwin, 1991; van der Veen *et al.*, 1999a, 1999b; Barnes *et al.*, 2006]. Signal noise is produced principally by postdepositional processes such as wind-driven snow deposition/erosion processes (for example, sastrugi). Additional error may be introduced during attempts to identify annual layers in an ice core. Inside East Antarctica, snow accumulation is from medium to low and often comparable to the roughness height in katabatic wind areas. Postdepositional noise primarily influences shorter timescales [Fisher *et al.*, 1985], while misidentification of annual layers leads to overestimation of accumulation in one year and underestimation in the previous or following year. Both kinds of noise/error reduce the temporal representativeness of ice core time series. Snow accumulation is also an important parameter for determining the net depositional flux of species (chemical/isotopic/dust) used as climatic and environmental markers [e.g., Fischer and Wagenbach, 1996]. Moreover, it is important to know ice core spatial representativeness with respect to a given time resolution.

[4] Accurate knowledge of the spatial distribution of snow accumulation is fundamental to understanding the

<sup>1</sup>Ente per le Nuove Tecnologie, l'Energia e l'Ambiente, Rome, Italy.

<sup>2</sup>Istituto Nazionale di Geofisica e Vulcanologia, Rome, Italy.

<sup>3</sup>Dipartimento di Scienze della Terra, University of Siena, Siena, Italy.

<sup>4</sup>Dipartimento di Ingegneria delle Strutture, dei Trasporti, delle Acque, del Rilevamento, del Territorio, University of Bologna, Bologna, Italy.

present, past, and future surface mass balance (SMB). It is also important in numerical simulations and atmospheric climate models used to reconstruct and forecast ice sheet dynamics and the study of implications for sea level change. Because of the large gaps in observations, any estimate of the current SMB will inevitably involve a large error [Genthon and Krinner, 2001; Frezzotti et al., 2004b]. The SMB is known to exhibit high spatial variability [e.g., Richardson et al., 1997; Frezzotti et al., 2005]. Frezzotti et al. [2004b] pointed out that snow precipitation is homogeneous on a large scale (hundreds of square kilometers), but wind-driven sublimation phenomena determined by the surface slope along prevailing wind directions (SPWD) have a considerable impact on the spatial distribution of snow over short (tens of meters) and medium (kilometer) spatial scales. It is known that sublimation in Antarctica is not negligible [e.g., Stearns and Weidner, 1993; Bintanja, 1998; Gallée, 1998; Gallée et al., 2001; van den Broeke et al., 2005], and methods for describing spatial and temporal variability must be further developed [Cullather et al., 1998]. The snowdrift process is not explicitly included in numerical weather forecasting and general circulation models [Gallée et al., 2001; Genthon and Krinner, 2001; Krinner et al., 2006]. One of the biggest areas of uncertainty regarding SMB is the role of surface and wind-driven sublimation [e.g., Genthon and Krinner, 2001].

[5] As pointed out by the *Ice Sheet Mass Balance and Sea Level (ISMAS)* [2004] Committee, accurate new field data on SMB on local and regional scales are required in order to characterize spatial and temporal variability and the representativeness of local records, and comparisons also need to be made over local (<10 km) and annual scales at selected sites.

[6] The variability of snow accumulation needs to be investigated over several spatial scales:

[7] 1. Surface micromorphology (for example, sastrugi, barchans, etc.) displays high variability in space (<1 km) and time (seasonal), and micromorphology (less than meter scale) significantly influences the core and stake records obtained on scales ranging from seasonal to multiannual.

[8] 2. Surface morphology and slope (determined by ice dynamics and bedrock topography) influence wind-driven ablation processes and determine a high variability of snow accumulation at medium scales between 1 and 20 km, thus influencing medium-depth core records.

[9] 3. Ice sheet morphology (determined by the accumulation rate history, its spatial pattern, and conditions at ice sheet boundaries) influences snow accumulation over very long scales between 20 and 200 km.

[10] Talos Dome (TD) is an ice dome on the edge of the East Antarctic plateau (Figure 1). In 2004 a new ice-coring project began at TD within the framework of the Talos Dome Ice Core Project (TALDICE). The aim was to retrieve 1550 m of ice spanning the last 120,000 years [Frezzotti et al., 2004a]. In order to provide detailed information on the temporal and spatial variability of snow accumulation, research was conducted at TD and along a north-south transect (GPR20-GV7-GV5-TD-31Dpt), within the framework of the International Trans-Antarctic Scientific Expedition (ITASE) program [Mayewski and Goodwin, 1999]. Oversnow traverses were conducted in 1996 (Terra Nova

Bay-Talos Dome; TNB-TD), 1998–1999 (Terra Nova Bay-Dome C; TNB-DC), and 2001–2002 (Wilkes Land-Victoria Land; D80-M4). The stake farms established during the traverses were resurveyed 1 to 7 times, using a Twin Otter aircraft, during the period 1996–2005.

[11] Along the traverses, stake-farm measurements, ice core analyses, and snow radar surveys were used to gain detailed insight into spatial (on a meter to kilometer scale) and temporal (on an annual to secular scale) variability in order to reconstruct temporal variability over the last 200 years and obtain information on secular spatial variability on scales ranging from a kilometer to hundreds of kilometers.

[12] This paper uses these results to provide new information regarding the impact of surface morphology on SMB on a meter (for example, sastrugi) and kilometer (for example, SPWD, transverse dune, wind crusts) scale and assess the ensuing implications for paleoclimatic reconstructions based on ice core studies and surface mass balance investigations. Moreover, the paper contributes to ongoing debate concerning the estimation of uncertainty in the measurement of spatial and temporal variability in snow accumulation and which records could be suitably compared with or used to verify atmospheric models and meteorological instrumental records.

## 2. Talos Dome Geographic, Morphological, and Meteorological Characteristics

[13] TD is located about 290 km from the Southern Ocean and 250 km from the Ross Sea (Figure 1). The 470-km-long transect follows the ice divide extending from the Southern Ocean (GPR20, 70°16'S; 158°18'E) to Talos Dome (TD, 72°48'S; 159°06'E) in a NNW-SSE direction, and then continues in a SW direction toward Taylor Dome (31Dpt, 74°02'S, 155°57'E) in the Ross Sea basin (Figures 1 and 2). The distance from the sea progressively increases between GPR20 (95 km) and Talos Dome (290 km), while remaining constant in the southern part at about 280 km from the Ross Sea.

[14] The transect starts at an elevation of 1587 m (all elevations in this paper were surveyed with a GPS system and are relative to the WGS84 ellipsoid) and reaches a maximum elevation at TD (2318 m), before descending to 2070 m at 31Dpt (Figure 2). The transect shows an overall upward slope from GPR20 up to 30 km south of TD. From this point to 31Dpt, it descends and cuts the contour lines at an angle of  $50 \pm 20^\circ$ . An analysis of the morphological conditions along the transect based on satellite images (Landsat 7 ETM+ and Radarsat) and the topography/slope profile [digital elevation model (DEM) from European Remote Sensing (ERS) radar altimeter] allows four sectors to be identified (Figure 2; the distance in kilometers is from GPR20):

[15] ● A 50-km-long steeply sloping area from GPR20 to GV7, characterized by slopes of up to  $80 \text{ m km}^{-1}$  (average  $7.5 \text{ m km}^{-1}$ ) with wind crusts and transverse dunes at the bottom of slope.

[16] ● An ice divide area extending from GV7 to 170 km from GPR20, with a slope of 2 to  $4 \text{ m km}^{-1}$ .

[17] ● A dome area extending from GV5 to 350 km from GPR20, with a slope generally  $<2 \text{ m km}^{-1}$ .

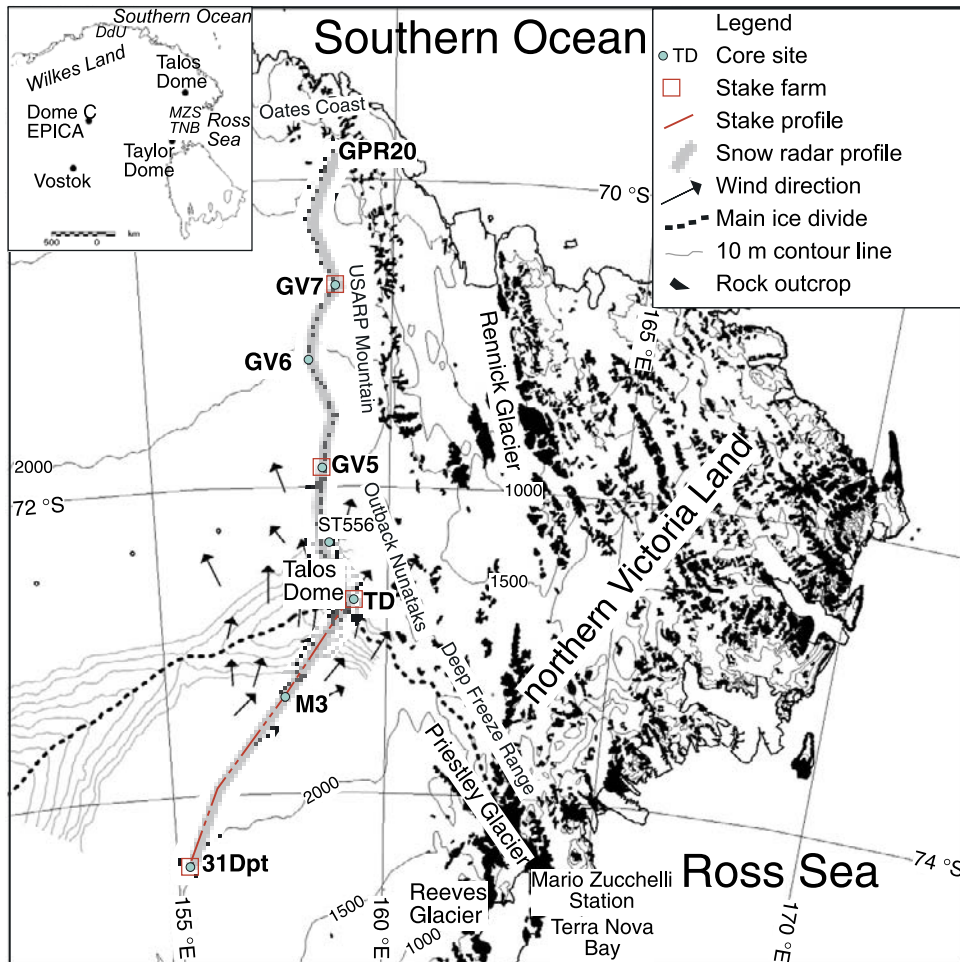


**Figure 1.** Location map of the Talos Dome area and the north-south transect showing core and stake-farm sites, snow radar and stake profiles, and wind direction from satellite images [Mancini and Frezzotti, 2003]. Contour lines are indicated every 500 m and every 10 m around Talos Dome (from Rémy et al. [1999]).

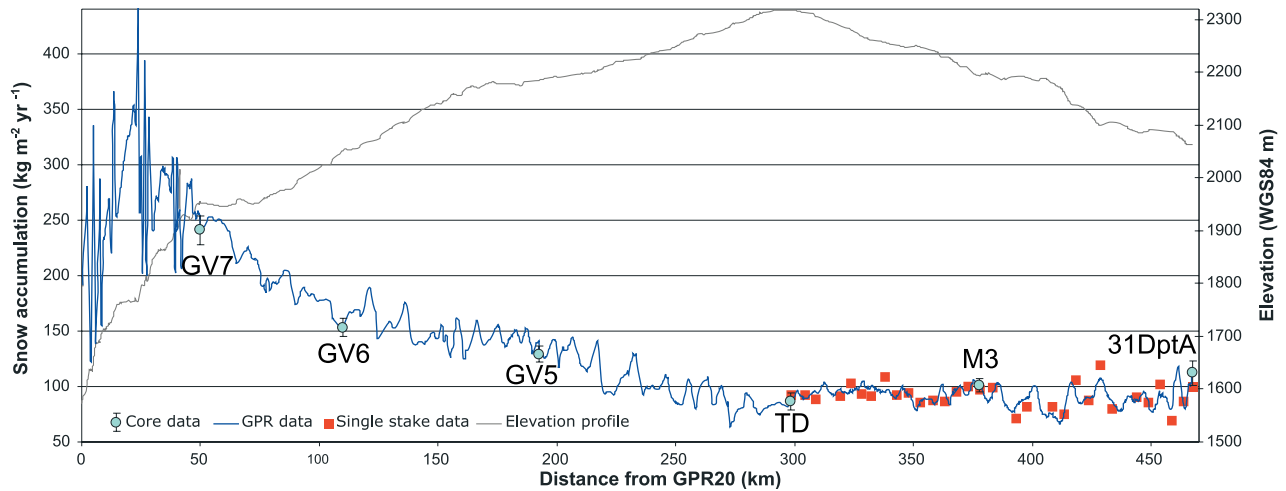


**Figure 2.** Topographic profile (from GPS) along the GPR20-GV7-GV5-TD-31Dpt transect (location shown in Figure 1) showing core (circle) and stake (square) sites and spatial distribution of snow accumulation from GPR layer 3 (dated to 1905 ± 9 AD) as well as ice core (from atomic bomb markers [Stenni et al., 2002; Magand et al., 2004]) and stake profiles (1996–2001 AD).

[18] • A plateau area with a slope of up to  $7 \text{ m km}^{-1}$  from M3 to 31Dpt.

[19] The surface morphology in the slope and plateau areas is very irregular and can be linked to flow over undulations in the bedrock morphology and, secondarily, to environmental conditions (wind and snow accumulation). In the dome and ice divide area, the surface morphology is smoother mainly to ice dynamics and environmental conditions and secondarily to bedrock morphology.

[20] Analyses of surface macromorphology and micro-morphology data obtained from satellite images and surface surveys show that the regions are swept by a weak to strong katabatic SW to SE wind, which drains cold air from the interior downslope to the Southern Ocean coast [Frezzotti *et al.*, 2002b; Mancini and Frezzotti, 2003]. Most of transect follows the ice divide and dome where the katabatic wind is weaker than in the adjacent wind confluence areas. These observations are generally consistent with streamline results from the katabatic wind field model simulation of Paris and Bromwich [1991]. Surface morphology surveys conducted during the traverses and satellite data analysis reveal that the prevailing wind direction follows the transect (SW-NE 31Dpt-TD; SSE-NNW from TD to GPR20). The topographic slope from 31Dpt to M3 is relatively high (up to  $7 \text{ m km}^{-1}$ ), but the wind direction closely matches that of the elevation contours; therefore the SPWD is low. The prevailing wind on the windward side (TD-M3) climbs the dome topography of TD with a SPWD of  $1\text{--}2 \text{ m km}^{-1}$ . The wind that reaches TD blows along the Rennick and Matusевич Glacier basins and forms several blue ice areas. A blue ice area 40 km from TD (Frontier Mountain) is characterized by an ice ablation rate of  $65 \text{ kg m}^{-2} \text{ yr}^{-1}$  [Folco *et al.*, 2002] plus an ablation of total precipitation, which leads to a negative SMB of around  $150 \text{ kg m}^{-2} \text{ yr}^{-1}$ .

[21] Research conducted during 1998–1999 along the traverse between TNB-DC demonstrated that wind-driven sublimation processes, determined by SPWD, have a huge impact on snow accumulation [Frezzotti and others, 2002a, 2002b, 2004b, 2005]. In order to reduce the impact of wind-driven processes, the core sites during the 2001–2002 traverse (GV7, GV5) were selected to be on a flat area where katabatic wind action and strength were lower [Magand *et al.*, 2004]. A detailed analysis of ice cores and snow radar at the 31Dpt and TD sites showed low spatial variability in snow accumulation [Frezzotti *et al.*, 2004a, 2005].

[22] An analysis of firn temperature [Frezzotti and Flora, 2002; Magand *et al.*, 2004] reveals that temperature is strongly correlated with surface elevation between GV7 and TD, with a superadiabatic lapse rate [ $2.5^\circ\text{C} (100 \text{ m}^{-1}) R^2 = 0.97$ ], whereas the lapse rate between TD and 31Dpt is near-dry-adiabatic [ $1.0^\circ\text{C} (100 \text{ m}^{-1}) R^2 = 0.98$ ], similar to that observed along the TNB-DC transect. An analysis of chemical and isotopic snow variability along the traverses shows that the majority of precipitation along the GPR20-TD transect comes from the Southern Ocean, whereas along the TD-31Dpt transect, it comes from the Ross Sea area [Becagli *et al.*, 2004; Magand *et al.*, 2004]. Sea spray components show maritime air intrusion (from the Southern Ocean) from GPR20 to GV7 [Becagli *et al.*, 2004]. These atmospheric conditions are consistent

with the modeled flux of moisture into the Ross Sea-East Antarctic region [Cullather *et al.*, 1998].

### 3. Materials and Methods

#### 3.1. Stakes

[23] Between 1998 and 2001, at TD and along the ITASE traverse [Frezzotti *et al.*, 2005; Magand *et al.*, 2004], 17 stake farms were set up, each including from 30 to 60 stakes planted 100 m apart in the shape of a cross within an area of  $4 \text{ km}^2$ ; each cross was centered on a firn core site. The 3-m-long polycarbonate stakes were anchored at the bottom. Measurements were carried out up to seven times annually, with most stakes measured from two to four times. During 1996, on the ITASE traverse from TNB to TD [Frezzotti and Flora, 2002], aluminum stakes were installed at 5-km intervals to provide a profile, and nine stakes were placed 8 km from the center of TD. The stakes between 31Dpt and TD were partially remeasured in 1998 and totally in 2001. The accuracy of the stake height measurements was estimated to be  $\pm 20 \text{ mm}$  of snow. Density profiles were determined using samples taken from the walls of snow pits up to 2.5 m deep to obtain water equivalent values at each stake-farm site. The densities along the stake profile were measured in 1996 using samples taken from the walls of snow pits up to 1.5 m deep, located at 20-km intervals. The snow accumulation rate was calculated for each year or for a number of years assuming that the measured density profiles were valid and did not change over the measurement period (stake and density profile measurements were carried out between December and mid-January). Although snow compaction was not taken into account in the calculation of snow accumulation, it has often been found to be negligible at low accumulation sites [Lorius, 1983]. Here a detailed analysis of the stake-farm data (GV7, GV5, TD, 31Dpt) was carried out along the north-south transect that crosses TD. The results of the other stake farms have been presented in part in other papers [Magand *et al.*, 2004; Frezzotti *et al.*, 2005] and will also be discussed here. The annual accumulation in  $\text{kg m}^{-2} \text{ yr}^{-1}$  at GV7, GV5, TD, and 31Dpt stake farms is an indicator of the interannual variability and annual spatial variability. The large annual standard deviation reflects the surface morphology (for example, sastrugi, barchans, etc.) and indicates that there is a limit to the degree to which a single stake (or firn core) value may be considered to be spatially representative. Multiannual variability is substantially lower than annual variability, suggesting that spatial variability may be reduced by increasing the time averaging interval [e.g., Palais *et al.*, 1982; Petit *et al.*, 1982; Mosley-Thompson *et al.*, 1995; Dibb and Fahnestock, 2004].

#### 3.2. Cores

[24] Starting from 1996, during the traverses [Stenni *et al.*, 2002; Magand *et al.*, 2004; Frezzotti *et al.*, 2005], 10 snow-firn cores (from 12 to 89 m deep) were drilled at sites between GV7 and 31Dpt at intervals of 60–80 km (Figure 1 and Table 1) using an electromechanical drilling system (10-cm diameter). Three cores were drilled at 31Dpt (31DptA, 31DptB, and 31DptC, from 48 to 7 m deep) and two at TD (89 and 55 m deep), 5–7 km apart. Snow temperature profiles were measured down to a depth

**Table 1.** Location of Coring Sites and Compilation of Accumulation Rates and Temperature Data<sup>a</sup>

Site	Long. E	Lat. S	Elev.	Dist.	T	IV	Stakes	Accumulation Rate kg m <sup>-2</sup> yr <sup>-1</sup>				
								1965–Pres.	1816–Pres.	1816–1965	Bot.–Pres.	Bot.
GV7	158°52'	70°41'	1947	95s	-31.8	0.3 ± 0.01	252 (3 yr)	241 ± 13 <sup>b</sup>	–	234	237 (1854)	239 (1854–1874)
GV6	158°17'	71°11'	2048	140s	-34.4	–	–	153 ± 8 <sup>b</sup>	–	–	–	–
GV5	158°32'	71°53'	2184	200s	-36.9	0.3 ± 0.01	135 (3 yr)	129 ± 7 <sup>b</sup>	129	129	128 (1776)	143 (1776–1796)
ST556	158°45'	72°22'	2246	240s	-38.1	–	–	101 <sup>c</sup>	–	–	105 <sup>c</sup> (1902)	–
TDN	159°05'	72°46'	2316	250r	-41.5	0.1 ± 0.01	74 (4 yr)	–	83.6	–	–	–
TD	159°06'	72°48'	2316	250r	-41.5	0.04 ± 0.01 <sup>d</sup>	81 (8 yr)	86.6 <sup>c</sup>	83.6 <sup>c</sup>	84	80 <sup>c</sup> (1231)	78 <sup>c</sup> (1231–1259)
M3	157°40'	73°23'	2203	240r	-43.2	1.9 ± 0.01	98 (7 yr)	101 ± 6 <sup>b</sup>	–	–	–	–
31 DptA	155°58'	74°02'	2069	240r	-41.8	7.97 ± 0.04 <sup>e</sup>	98.7 (6 yr)	112 ± 5.6 <sup>b</sup>	98 ± 4.9 <sup>d</sup>	98	101 (1723)	96 (1723–1743)
31 DptB	156°00'	74°04'	2040	240r	-41.8	–	–	137 ± 14 <sup>b</sup>	–	–	–	–

<sup>a</sup>Elev. = Elevation WGS84 in meter; Dist. = Distance from coast (km); T = Firm Temperature (°C); IV = Ice velocity by GPS m yr<sup>-1</sup>; Pres. = Present; Bot. = Age at bottom core; s = Southern Ocean; r = Ross Sea.  
<sup>b</sup>Magand et al. [2004].  
<sup>c</sup>Stenni et al. [2002].  
<sup>d</sup>Frezzotti et al. [2005].  
<sup>e</sup>Vitucci et al. [2004].

of 30 m at the core sites after a 15- to 24-hour equilibration period [Frezzotti and Flora, 2002; Magand et al., 2004]. Snow/firn density was determined immediately after retrieval by measuring and weighing core sections. Snow was poorly sintered in the uppermost layers; densities for these layers were therefore measured in a pit (close to the main core and stake farm) where stratigraphic studies and snow sampling were also performed.

[25] The radioactive reference horizons from 1965 and 1966 atmospheric thermonuclear bomb tests were used to determine the mean accumulation rate over the last 50 years of all the cores [Stenni et al., 2002; Magand et al., 2004; Frezzotti et al., 2005]. To determine the mean accumulation rate at 31DptA, Frezzotti et al. [2005] used the volcanic sulfate signals of the Tambora eruption (1815 AD) and an unknown volcanic event (1809 AD). Whereas to evaluate the accumulation variability of TD and ST556 cores, Stenni et al. [2002] used the seasonal variation in nssSO<sub>4</sub><sup>2-</sup> and NO<sub>3</sub><sup>-</sup> concentrations, coupled with the identification of atomic bomb markers and nssSO<sub>4</sub><sup>2-</sup> spikes from the most important past volcanic event. Using the same method as Stenni et al. [2002], we evaluated the temporal accumulation variability of GV7, GV5, and 31DptA cores. Dating error was due to incorrect identification of missing seasonal nssSO<sub>4</sub><sup>2-</sup> signals and incorrect identification of errors in volcanic chronology. Dating error should generally be around ±1 year near historical volcanic markers and may reach ±5 years (for the low accumulation sites such as TD) at points that are far from dated reference horizons (volcanic and atomic bomb markers). We did not take into account layer thinning due to vertical strain since the ratio of core depths (maximum 89 m) to the entire thickness of the ice (from 1500 m to more than 3000 m) is less than 5% and vertical strain is therefore negligible. Horizontal ice velocities measured by GPS at core sites were between 2 and 8 m yr<sup>-1</sup> along the southern transect (M3 and 31Dpt) and less than a few decimeters per year along the ice divide from TD to GV7 (Table 1 [Vitucci et al., 2004; this paper]). The maximum horizontal distance that a snow layer can be transported downstream subsequent to deposition varies from 1780 m for the deeper part of 31DptA to 66 m for GV5 and GV7 and much less for TD. Spatial variability of snow accumulation at 31Dpt was very low [Frezzotti et al., 2005] and negligible at the other sites.

[26] The experimental error (±σ<sub>e</sub>) in the calculated snow accumulation rates for the different periods is estimated to be less than 10% for β radioactivity (1955/1965–1998), about 10% for the unknown-Tambora period (1810–1816), and less than 5% for the tritium-present (1966–1998) and Tambora-present (1816–1998) periods [Stenni et al., 2002; Magand et al., 2004; Frezzotti et al., 2005]. These values take into account the different sources of error linked to density determination and the sampling resolution (20–40 cm for β, 3–5 cm for tritium, 2.5–4 cm for SO<sub>4</sub><sup>2-</sup>).

### 3.3. Geophysical Measurements

[27] Internal layers of strong radar reflectivity observed with ground-penetrating radar (GPR) are isochronous, and surveys along continuous profiles provide detailed information on the spatial variability of snow accumulation [e.g., Richardson et al., 1997; Vaughan et al., 1999; Arcone et al., 2004; Eisen et al., 2004; Spikes et al., 2004]. These

horizons result from dielectric contrast associated with chemical and crystal fabric changes. The integration of global positioning system (GPS) and GPR data yields the ellipsoidal height of both the topographic surface and firn stratigraphy (Table 1 and Figure 2). GPS and GPR surveys and subsequent analyses are described elsewhere [Frezzotti *et al.*, 2002a]. Data acquisition was performed with a GSSI Sir10B unit equipped with one monostatic antenna with a central frequency of 200 MHz.

[28] The traces were recorded at about 1 scan  $m^{-1}$  in a 750-ns time window for a 60 to 70 m investigation depth. A scan rate of 4 scans  $s^{-1}$  was used with 512 samples per trace. Postprocessing of GPR data involved gain ranging, low and high band-pass filtering, and trace stacking. The recorded two-way traveltimes (TWT) were converted to depths using the methodology based on density-depth information outlined by Frezzotti *et al.* [2002a]. Density information was obtained using the 10 firn cores (from 7 to 89 m deep) and 5 snow pits (2.5 m deep). All density data were fitted with a second-order polynomial function for transect, yielding a correlation coefficient ( $R^2$ ) of more than 0.9 for measured and computed densities.

[29] The GPR pulse duration (8 ns) yields a vertical interface resolution of about 60 cm in firn with a refractive index of  $n = 1.5$  (density of  $500 \text{ kg m}^{-3}$ ). However, depth accuracy is also affected by uncertainties in the GPR TWT depth-layer age conversion, layer tracking (about 10–20 cm), and density measurements. Depth uncertainty in GPR data was estimated to be about  $\pm 14$  cm for the data acquired.

[30] Three internal layers were chosen and tracked along the transect. In this paper, the profiles of the deepest, continuously traceable layers identified (layer 3, L3) are shown in Figure 2 and discussed in detail below. On the basis of the depth-age function and depth of layers at GV7, GV5, TD, and 31Dpt, layer 3 was dated to  $1905 \pm 9$  AD.

[31] Surface elevation profiles and local topography along the traverse were measured by GPS, whereas regional surface topography was analyzed using a DEM of Antarctica provided by Rémy *et al.* [1999]. The DEM was created with a 1-km grid size using a radar altimeter from the ERS satellite. The DEM has an accuracy of better than 1 m over the portions of East Antarctica where slope gradients are less than 0.5% (the transect between GPR20 to GV7 displays a slope above this threshold). Geodetic Trimble 4000 ssi and 5700 dual-frequency receivers were used for kinematic surveys; high sampling rates (GPS sample rate at 1 s) were adopted to allow a detailed survey of elevation profiles. Vehicle and thus antenna speed oscillated from about 12 to 16  $\text{km h}^{-1}$ , corresponding to 1 scan every 3–4 m.

[32] The GPS data were processed using the precise point positioning (PPP) technique [Neilan *et al.*, 1997; Zumbege *et al.*, 1997]. Zumbege *et al.* [1997] have shown the validity of their approach by analyzing daily sets of carrier phase data achieving a millimeter level of repeatability in the horizontal components and centimeter precision in the vertical direction [Gandolfi *et al.*, 2005; Negusini *et al.*, 2005].

[33] The accuracy of the elevation profile along the traverse was around 10–20 cm; this is sufficient considering the presence of boundary problems, such as the pressure of

the track on the snow surface, which could lead to a similar or even higher degree of uncertainty. Solutions using a reference station and differenced solutions present far more logistical problems both during surveying and data processing. As for kinematic surveying, certain conditions made it impossible to obtain a solution for some short tracks. In order to provide a continuous profile between GPR20 and 31Dpt, it was necessary to fill in the data gaps using ERS data with some correction. Taking into account the different accuracies of the GPS profile (a few centimeters) and the ERS data set (around 1 m), the only solution was to perform an ad hoc adaptation of the ERS data over the GPS profile at the boundary of data gaps. The new data set obtained (latitude, longitude, and ellipsoidal height), representing the entire continuous profile, was associated with a different root mean square (RMS) error for the height derived by GPS and for the height derived by ERS. In particular, the real RMS error obtained using the PPP solution was associated with the GPS point, and a conventional RMS error at the meter level was associated with the adapted ERS data.

## 4. Results and Discussion

### 4.1. Spatial Variability on a Local Scale

[34] The rate of stake burial is often referred to as accumulation, whereas the emergence of a stake (or no change in its height) can be caused by wind scour, sublimation, and/or compaction of snow between the surface and the depth at which the stake is anchored in the snow (1–2 m). Stake height decreases over time because of snow precipitation and transport, and increases because of wind scour, sublimation, and compaction of snow [Dibb and Fahnestock, 2004]. The accumulation/ablation pattern emerging from the stake-farm measurements makes it possible to survey the annual accumulation value and noise on an annual scale by comparing the variations in the accumulation at each stake with the average across the stake farm. The detected “noise” represented by the standard deviation of the measured values, is high and largely reflects the snow surface roughness (sastrugi). It limits the degree to which a single annual snow accumulation value observed in a core may be considered to be representative. The snow surface is irregular and changes because of redistribution processes.

[35] The surface morphology, characterized by sastrugi, barchans, etc., is similar at the GV7, GV5, TD, and 31Dpt sites, which exhibit surface irregularity with an average roughness height of 20 cm and maximum of 40 cm. Surface surveys have shown that maximum morphology irregularity and hardness occur at the beginning of the summer season (October to mid-November), whereas irregularity and hardness reach a minimum at the end of the summer season (end of January). During the summer season, these morphological characteristics are slowly leveled by sublimation, densification processes, deflation, and redeposition, resulting in the slow filling of hollows and erosion of peaks [e.g., Gow, 1965; Goodwin, 1991].

[36] At sites where stake measurements showed accumulation of less than  $120 \text{ kg m}^{-2} \text{ yr}^{-1}$  (TD and 31Dpt), zero or negative accumulation values have been observed for individual stakes. Stake measurements and surface morphology

**Table 2.** Temporal Variability of Snow Accumulation From Stake Farms<sup>a</sup>

Year	GV7 (N 31)			GV5 (N 31)			TDN (N 60)			TD (N 9)			31Dpt (N 36)		
	ACC	SD	DIF	ACC	SD	DIF	ACC	SD	DIF	ACC	SD	DIF	ACC	SD	DIF
1996–1998										82	28	94			
1998–2000													105	22	94
2000–2001										82 <sup>b</sup>	18 <sup>b</sup>	95 <sup>b</sup>	96	54	85
2001–2002	290	11	120	145	17	113	125	40	144				96	46	86
2002–2003	113	42	47	109	52	84	62	77	72				133	40	119
2003–2004	352	12	146	151	26	117	60	79	69	80 <sup>c</sup>	19 <sup>c</sup>	92 <sup>c</sup>	61	59	54
2004–2005							52	79	60						
Multi-annual	252	5	104	135	16	105	74	14	85	81	12	94	99	7	88

<sup>a</sup>N = Number of stakes; ACC = Accumulation rate  $\text{kg m}^{-2} \text{yr}^{-1}$ ; SD% = Standard deviation %; DIF = Difference in percent between stakes value and 50 years average.

<sup>b</sup>1998–2002.

<sup>c</sup>2002–2004.

appear to be strongly related at all sites, as was previously noted along the TNB-DC traverse [Frezzotti et al., 2005]. At the South Pole, stake-farm analysis and meteorological conditions on a monthly scale have been used to correlate stake standard deviation to wind transport [McConnell et al., 1997]. The annual average value of the standard deviation is about  $45 \text{ kg m}^{-2} \text{yr}^{-1}$ , representing the average noise introduced by sastrugi (Table 2). The lowest standard deviation values are found when the SPWD is low and accumulation is high. Along the TNB-DC transect, the presence of a wind crust at the surface is strongly correlated with a high standard deviation and zero or negative accumulation. The site with high SPWD variability shows the lowest accumulation values and the highest standard deviation (144%), with accumulation  $\leq 0$  for a 5-year period in 40% of cases [Frezzotti et al., 2005]. A low level of annual noise occurs at the site with the highest accumulation, GV7 (standard deviation of 11–12%), whereas the highest level of noise occurs at TD (standard deviations of up to about 80%).

[37] Frequency analysis of single stake (or single core) accumulation measurements compared to annual average accumulation shows that the data are not representative on an annual scale, even for the site with the highest accumulation (GV7). On an annual scale, the accumulation distribution graph (Figure 3) shows that more than 80% of the stakes at TD and more than 40% of the stakes at GV7 show accumulation differences of more than  $\pm 10\%$  compared to the average. Representativeness increases with multiyear averages: accumulation at GV7 is representative within  $\pm 10\%$  using three cumulative years and at other sites (GV5, TD, and 31Dpt) using at least seven cumulative years. This is confirmed by Goodwin et al. [2003], who consider the 3-year running mean accumulation data of eastern Wilkes Land ice core (from  $235$  to  $570 \text{ kg m}^{-2} \text{yr}^{-1}$ ) to be representative of the precipitation minus evaporation, whereas 1-year accumulation data reflect precipitation plus the local microrelief noise. Figure 4 shows the percentage of points for which the accumulation difference compared to the mean value was less than  $\pm 10\%$ , as well as the mean annual accumulation values for each site and for each set of measurements. The very good correlation ( $R^2 = 0.82$ , significance level  $>99\%$ ,  $n = 101$ ) and the assumption that postdepositional phenomena are systematic noise components due to meteorological and morphological site characteristics have led us to conclude that only sites with more than  $750 \text{ kg m}^{-2} \text{yr}^{-1}$  give representative values ( $\pm 10\%$ ) on an annual scale. For South

Pole, McConnell et al. [1997] computed the average time (310 years) required to statistically ensure that each monthly snow accumulation record within the year is adequately represented in the time average. The authors also pointed out that the averaging of adjacent cores would decrease the time window proportionally. van der Veen et al. [1999a] argued that noise could be removed using a Gaussian weighting function with a standard deviation of about 5 years. The South Pole and TD show very similar accumulation values ( $85 \text{ kg m}^{-2} \text{yr}^{-1}$ ) and are also similar in terms of the number of years required to ensure a well-represented annual value (about 7 years on the average). Sites with accumulation values of less than  $750 \text{ kg m}^{-2} \text{yr}^{-1}$  are representative if cumulative accumulation data computed over a number of years are used to reach this threshold (for example, 3 years for  $250 \text{ kg m}^{-2} \text{yr}^{-1}$ , 7–8 years for  $100 \text{ kg m}^{-2} \text{yr}^{-1}$ ) or a multicore approach is adopted.

[38] A major problem in establishing accurate annual or seasonal stratigraphy in firn/ice cores is the possibility that some annual/seasonal layers may be missing in the stratigraphic record. Stake-farm measurements and ultrasonic height multi-instruments are the best way to detect zero accumulation or erosion values on an annual or seasonal scale. This information cannot be obtained by ice core analysis. At the South Pole, the frequency distribution of stratigraphic layer thicknesses in cores and in a snow pit is not compatible with a significant number (between 1% and 5% probability) of missing layers associated with zero-accumulation years inferred from pole-height measurements. The implication is that a large percentage of years (about 10%) are missing from the ice core stratigraphy [van der Veen et al., 1999b; Mosley-Thompson et al., 1995]. Comparison between stake and core values makes it possible to measure the frequency distribution and infer the probability of identifying missing layers and lowest and highest snow accumulation values in firn cores. The distribution differences with respect to the mean annual accumulation for stake measurements and firn cores are compared in Figure 5 for each site. The distribution patterns between stakes and cores are clearly similar only at GV7. At sites with lower accumulation (GV5, TD, and 31Dpt), the stake value shows flatter distributions. The difference between core and stake measurements, at sites with accumulation lower than  $200 \text{ kg m}^{-2} \text{yr}^{-1}$ , could be attributed to misidentification of annual layers from seasonal signals and consequent errors in the definition of high and low values (values with differences  $>40\%$  compared to the average value). High annual peaks could be interpreted as a double

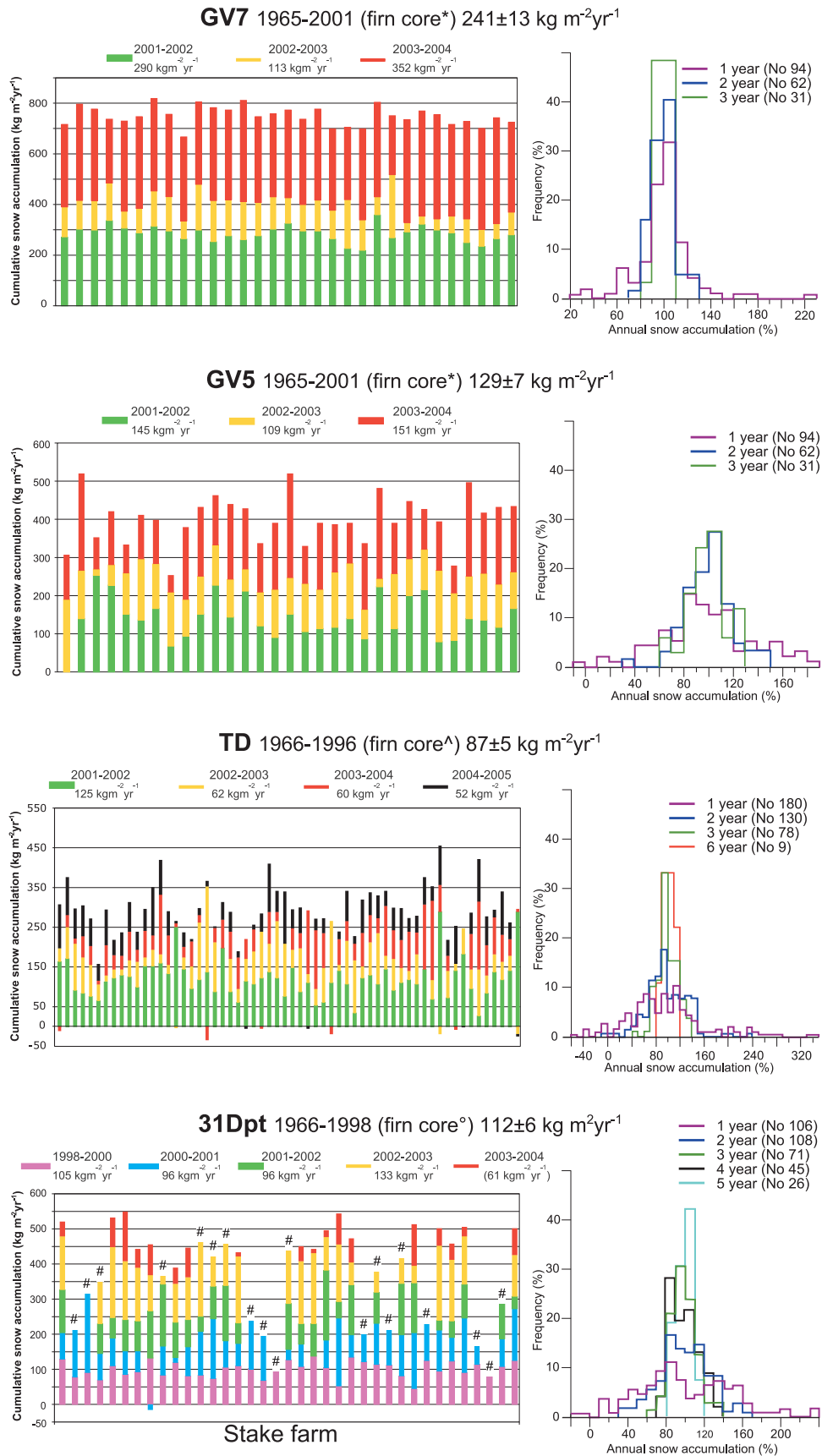


**Figure 3.** Accumulation/ablation pattern from stake-farm (GV7, GV5, TD, 31Dpt) measurements and frequency analysis of accumulation with respect to annual average accumulation. #Stake broken by wind. ^Stenni et al. [2002]; \*Magand et al. [2004]; °Frezzotti et al. [2005].

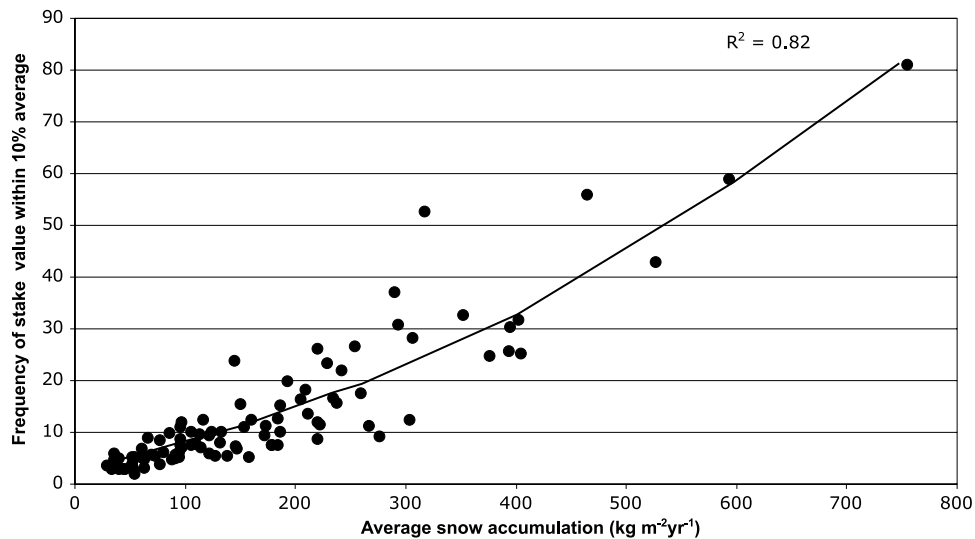


**Figure 4.** Frequency of stake values within 10% of the stake-farm mean value versus snow accumulation along the ITASE traverse [see also *Magand et al.*, 2004; *Frezzotti et al.*, 2005]. The curves correspond to the second-order regression function.

year and two adjacent peaks will not be stratigraphically detectable if they are sufficiently narrow and could therefore be interpreted as a single year.

**4.2. Spatial Variability on a Regional Scale**

[39] Along the transect from TD to 31Dpt, a comparison of snow accumulation from GPR ( $96 \pm 9$  year average) and single stake measurements (5-year averages) shows a similar pattern of accumulation with differences of around 10% (Figure 2). Differences are within instrumental error (density variation), and temporal and spatial differences among sample areas are also due to GPR soundings that were not carried out exactly over the stake; in some cases, the distance between the stake site and the snow radar survey exceeded 50 m. Consistently with the snow accumulation variability observed using snow radar, the highest difference between stake and GPR values and the highest variation in stake values may be observed in the area between M3 and 31Dpt, where accumulation variability of up to  $40 \text{ kg m}^{-2} \text{ yr}^{-1}$  over a distance of 5 km has been detected.

[40] An analysis of GPR measurements shows that maximum accumulation values, not correlated with transverse dunes (see Figure 6 and below), are to be found 30 km north of GV7 ( $350 \text{ kg m}^{-2} \text{ yr}^{-1}$ ). Between this point and

TD and GPR20, accumulation decreases progressively. Snow radar profiles show an increase in accumulation in the first 20 km from GPR20 and then a decreasing accumulation trend from the coastal area (GPR20) to about 25 km north of TD (downwind area), where the lowest values occur ( $65 \text{ kg m}^{-2} \text{ yr}^{-1}$ ). From TD to 31Dpt, in spite of decreasing elevation (from 2318 to 2070 m), only a slight increase in snow accumulation occurs (from 85 to  $115 \text{ kg m}^{-2} \text{ yr}^{-1}$ ). At the same elevation, the accumulation along the northern transect (GPR20-TD) reaches  $180 \text{ kg m}^{-2} \text{ yr}^{-1}$ . The first 50 km south of TD (TD-M3) shows the lowest variability in accumulation with values ranging from 95 to  $100 \text{ kg m}^{-2} \text{ yr}^{-1}$ . Between M3 and 31Dpt, and between 25 km north of TD and GV7, the snow accumulation profile shows clear variations in accumulation (up to  $40 \text{ kg m}^{-2} \text{ yr}^{-1}$  within 5 km). These high variations in accumulation are very well correlated with surface slope change. Accumulation decreases when the slope increases, mainly because of ablation driven by katabatic winds [*Frezzotti et al.*, 2004b, 2005]. In the slope area from GPR20 to GV7, these variations reach values of more than  $200 \text{ kg m}^{-2} \text{ yr}^{-1}$  within 1 km (from 123 to  $335 \text{ kg m}^{-2} \text{ yr}^{-1}$ ). At the transverse dunes site, the lowest accumulation value has been found at the highest slope (more than  $10 \text{ m km}^{-1}$ ), and

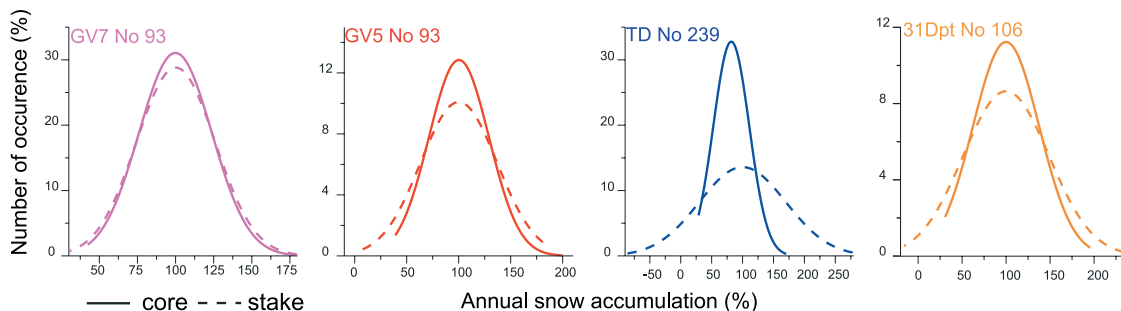


**Figure 5.** Analysis of the Gaussian distribution of annual accumulation values from single stakes versus the snow accumulation values from firm cores at each site and core and stake-farm time series.

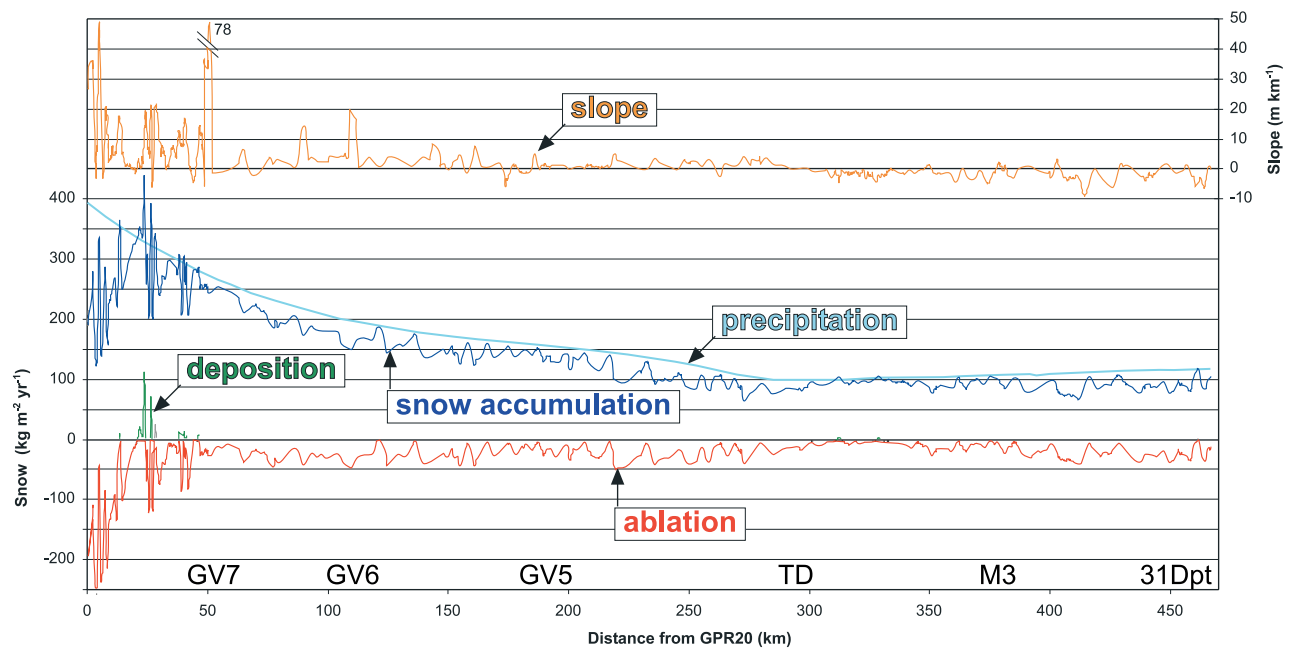


**Figure 6.** Transect spatial distribution of surface mass balance components and slope profile. Snow accumulation (SMB) from GPR data, precipitation (evaluated using a function of maximum value of GPR SMB, firm temperature, and coastal distance), ablation (precipitation-SMB), and deposition (value of excess precipitation at site). Slopes were calculated using the GPS profile along the transect. The direction of the prevailing wind follows the transect direction (SW-NE from 31Dpt to TD; NNW-SSE from TD to GPR20); therefore the profile generally represents the slope along the wind direction (SPWD).

the highest accumulation occurs at the bottom of slope. These morphologies have been observed by satellite measurements and during surveys along the TNB-DC traverse [Frezzotti *et al.*, 2002b] in sporadic areas between 2200 and 3000 m, mainly downwind of the wind crust area, where the surface decreases in slope. Transverse dunes usually consist of one or two dunes (with amplitude of a few meters and wavelength of around 5 km) perpendicular to the wind and slope direction and are characterized by sastrugi of more than 2 m in height. They are similar to those described by Black and Budd [1964] in Wilkes Land.

[41] The accumulation pattern in the dome area is asymmetrical with higher accumulation and lower variability in the southern sector (TD-M3) as compared to the northern sector (GV5-TD). These differences could be correlated with lower wind velocities in the southern sector due to positive slope gradients and reduced wind-driven sublimation [Frezzotti *et al.*, 2004a], whereas the lower accumulation and higher variability in the downwind sector is likely due to higher wind-driven sublimation determined by the increase in surface slope toward the Southern Ocean.

[42] On the basis of a previous analysis, the transect may be divided into five sectors (Figure 2 and Table 3):

[43] • Slope area from GPR20 to GV7, characterized by an average value of  $266 \text{ kg m}^{-2} \text{ yr}^{-1}$ , a standard deviation of 21%, and the highest variability (max  $441 \text{ kg m}^{-2} \text{ yr}^{-1}$ ; min  $122 \text{ kg m}^{-2} \text{ yr}^{-1}$ ).

[44] • Area from GV7 to the 150-km point (distance from GPR20) with an average value of  $184 \text{ kg m}^{-2} \text{ yr}^{-1}$ , a standard deviation of 17%, and moderate variability (max  $253 \text{ kg m}^{-2} \text{ yr}^{-1}$ ; min  $138 \text{ kg m}^{-2} \text{ yr}^{-1}$ ).

[45] • Area from the 150-km point to TD with an average value of  $118 \text{ kg m}^{-2} \text{ yr}^{-1}$ , a standard deviation of 22%, and moderate variability (max  $161 \text{ kg m}^{-2} \text{ yr}^{-1}$ ; min  $64 \text{ kg m}^{-2} \text{ yr}^{-1}$ ).

[46] • Dome area from TD to the 348-km point with an average value of  $95 \text{ kg m}^{-2} \text{ yr}^{-1}$ , the lowest standard deviation (5%), and low variability.

[47] • Area from the 348-km point to 31Dpt with an average value of  $90 \text{ kg m}^{-2} \text{ yr}^{-1}$ , a standard deviation of 11%, and moderate variability (max  $118 \text{ kg m}^{-2} \text{ yr}^{-1}$ ; min  $67 \text{ kg m}^{-2} \text{ yr}^{-1}$ ).

[48] Noone *et al.* [1999] found that precipitation reflects large (synoptic) scale phenomena related to circulation on a global scale. Several authors have demonstrated the dependence of SMB on temperature, elevation, saturation vapor pressure, and distance from the open ocean (continentality [e.g., Muszynski and Birchfield, 1985; Giovinetto *et al.*, 1990; Fortuin and Oerlemans, 1990]). Frezzotti *et al.* [2004b] pointed out that along the Dumont d'Urville-Dome C and TNB-DC transects, the maximum value of snow accumulation (not correlated with transverse dunes) is very highly correlated with firm temperatures and represents the snow precipitation minus surface sublimation induced by solar radiation (ablation not induced by wind). These authors concluded that the difference between the maximum and minimum SMB value at the site mainly reflects ablation processes driven by katabatic winds (wind-driven sublimation). Similarly the maximum snow accumulation values obtained from GPR soundings are very well correlated ( $R^2 > 0.97$ ) with firm temperature and coastal

**Table 3.** Surface Mass Balance Components<sup>a</sup>

Profile	Surface Mass Balance				P-SS	DEP	Wind-driven Sublimation			
	(kg m <sup>-2</sup> yr <sup>-1</sup> )			%			(kg m <sup>-2</sup> yr <sup>-1</sup> )		%	
	Ave	Min.	Max				SD	Ave	Max	WS/P-SS Ave
GPR20-GV7	266	122	441	21	332	14	66	260	20	68
GV7-150 km	184	138	253	17	211	0	28	48	13	24
150 km-TD	118	64	161	22	140	0	22	50	16	39
TD-348 km	95	82	105	5	101	1	7	17	7	17
348 km-31Dpt	90	67	118	11	111	0	21	43	19	39

<sup>a</sup>P-SS = Precipitation minus surface sublimation (kg m<sup>-2</sup> yr<sup>-1</sup>) calculated using the correlation between the maximum value of SMB from GPR, firm temperature and distance from the coast; DEP = Deposition Max value (kg m<sup>-2</sup> yr<sup>-1</sup>) calculated as excess value of the SMB minus P-SS; Wind-driven Sublimation (WS) has been calculated as P-SS minus SMB from GPR.

distance. On the basis of this correlation, the values of snow precipitation (P) minus surface sublimation (SS) induced by solar radiation during summer (P-SS) have been calculated along the transect (Figure 6). Using calculated P-SS values and the SMB provided by GPR, it is possible to estimate the ablation (P-SS minus SMB) and deposition (amount in excess of P-SS at the corresponding site). P-SS decreases significantly in the first 150 km (from 390 to 160 kg m<sup>-2</sup> yr<sup>-1</sup>), then remains at around 100–140 kg m<sup>-2</sup> yr<sup>-1</sup> up to 31Dpt. An analysis of the deposition distribution shows (Figure 6) that these phenomena are present only north of GV7 at transverse dune sites and are negligible (maximum value of 14 kg m<sup>-2</sup> yr<sup>-1</sup>) compared to ablation. On the basis of an atmospheric model, *Déry and Yau [2002]* estimated that the deposition process is about 2 orders of magnitude less important than wind-driven sublimation. The prevailing wind essentially follows the same direction as the transect. The slope along the prevailing wind direction (SPWD) was calculated using the average slope measured 3 km upwind. A comparison of SPWD and ablation profiles using AnalySeries 2.0.3 [*Paillard et al., 1996*] shows a negative correlation ( $R = -0.58$ , 99% significance level). Taking into account that the slope profile along the transect does not exactly follow the katabatic wind streamlines of surface airflow (differences up to  $\pm 20^\circ$ ), and also bearing in mind the uncertainty in P-SS values, we believe that wind-driven sublimation is very well correlated with SPWD. This negative correlation confirms a previous analysis conducted in a megadune area and at core sites along the TNB-DC and DdU transects [*Frezzotti et al., 2002a, 2004a*].

[49] An analysis of ablation values with respect to other SMB parameters reveals the following (Figure 6 and Table 3):

[50] • Wind-driven sublimation values are less than about 50 kg m<sup>-2</sup> yr<sup>-1</sup> from GV7 to 31Dpt; values up to 260 kg m<sup>-2</sup> yr<sup>-1</sup> are found only in the first 50 km (from GPR20 to GV7).

[51] • Average wind-driven sublimation values vary from 66 to 7 kg m<sup>-2</sup> yr<sup>-1</sup>, accounting from 7% to 20% of the P-SS of the entire profile.

[52] • From the 150-km point to TD and from the 348-km point to 31Dpt, wind-driven sublimation values equivalent to 30–40% of P-SS are reached frequently, and values higher than 40% of P-SS are reached along the northern part of the transect (first 25 km from GPR20).

[53] • Wind-driven sublimation reaches its maximum (260 kg m<sup>-2</sup> yr<sup>-1</sup>) between GPR20 and GV7, whereas the minimum value is between TD and 340 km in the dome area.

[54] • Maximum wind-driven sublimation values account for 68% of P-SS at the corresponding site.

[55] • Both wind-driven sublimation values (average and maximum) are very significant for the SMB calculation.

[56] • Wind-driven sublimation is well correlated with SPWD.

[57] Satellite image analysis of wind crust distribution and sastrugi fields shows that the transect crosses an area where the effect of katabatic winds is moderate or weak (ice divide and dome area). Dry air advection, and thus sublimation, is enhanced in areas where katabatic winds are strong and have a large downslope component [*van den Broeke, 1997*]. In spite of the fact that the transect is not in a katabatic wind confluence area and does not have an extensive wind crust area, unlike most of the adjacent area of East Antarctica, wind-driven sublimation is still a very important component of SMB with an average value amounting to 20% (from 66 to 7 kg m<sup>-2</sup> yr<sup>-1</sup>) of P-SS. Blowing snow sublimation driven by katabatic winds (wind-driven sublimation) is more effective than surface sublimation by solar radiation [*van den Broeke et al., 2004*]. However, surface sublimation has generally been estimated to be of the same order of magnitude as wind-driven sublimation [*Déry and Yau, 2002; van den Broeke et al., 2004*]. SMB studies using atmospheric models and automatic weather stations suggest that the two types of sublimation (surface sublimation and wind-driven sublimation) together account for the ablation of 20% of solid precipitation in Antarctica [*Déry and Yau, 2002; van den Broeke et al., 2004; Gallée et al., 2005*]. On the basis of the present results alone, wind-driven sublimation also accounts for 20% of P-SS in areas where the katabatic wind is from weak to moderate. Along the DdU-DC and TNB-DC traverse, *Frezzotti et al. [2004b]* estimated an average value of 75% for the wind-driven sublimation of P-SS, on a site where wind action has a greater impact and is characterized by an extensive wind crust presence.

### 4.3. Temporal Variability on an Annual and Secular Scale

[58] Repeated stake-farm (or multicore) measurements are the only way to detect annual/seasonal variations in snow accumulation in East Antarctica. Analyzing the current annual average values of stake farms makes it possible to

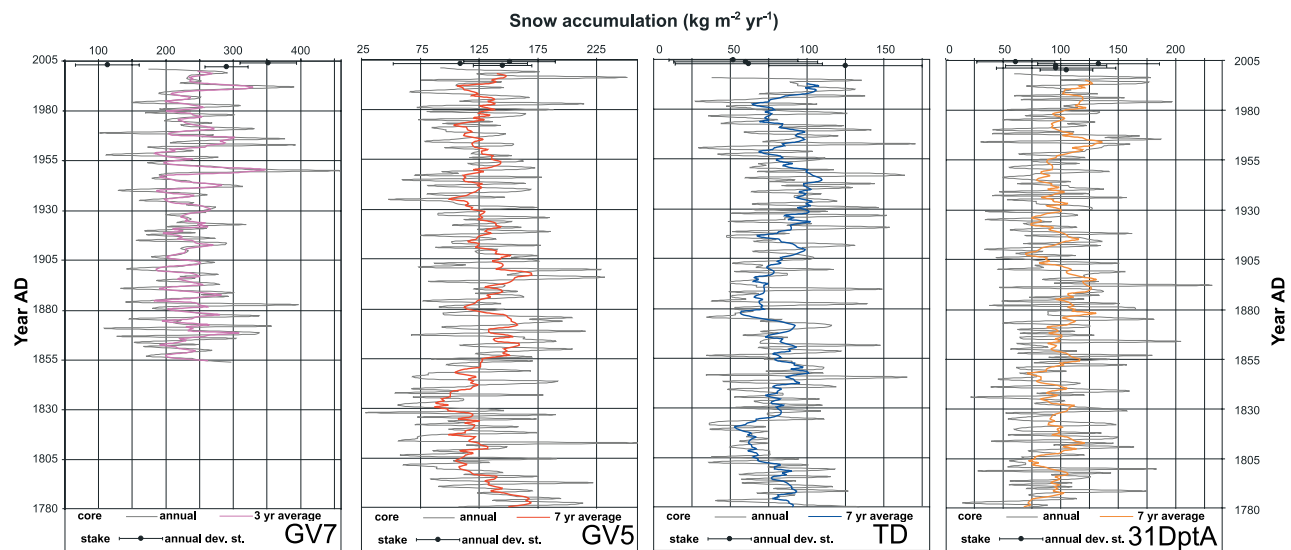


**Figure 7.** Time series of snow accumulation from firn cores at annual resolution (thin line) and 3-year (GV7) and 7-year (GV5, TD, 31DptA) average (solid line), and stake farms since 1780 AD.

monitor any changes in annual accumulation compared to decadal (50 years) or secular (200 years) timescale average from firn cores.

[59] Measurements from stake farms show different annual mean accumulation rates, with variations of up to nearly 50% compared to the 50-year average accumulation value estimated from firn cores (Table 2). Highest and lowest values occur at GV7 (site with the highest accumulation), which saw an increase to 146% during 2003–2004 and a reduction to 47% during 2002–2003. Core and stake-farm time series show an anomalous low accumulation value for the year 2002–2003 (Figures 3 and 7). GV7 and GV5 show the same pattern of increases and decreases in accumulation during the observation period (2001–2003), as do the other stake farms installed in Wilkes Land (D66, GV2, GV3, GV4 [see Magand *et al.*, 2004]). At these sites, accumulation was higher during 2001–2002 (with percentages ranging from 124% at GV2 to 106% at GV4) and lower during 2002–2003 (from 41% at GV2 to 87% at GV4), suggesting similar climatological conditions. TD, 31Dpt, and other sites along the TNB-DC traverse (MidPoint), where stake farms were installed and measured during 2001–2003, display different patterns of increases and decreases in accumulation.

[60] The 3-year stake accumulation average at GV5 and GV7 (2001–2004), 4- to 9-year average at TD (2001–2004; 1996–2004), and 6-year average at 31Dpt (1998–2003) show slightly higher values (104–105%) for GV5 and GV7 and lower values for TD and 31Dpt (85–94%; 88%) compared to the 50-year average accumulation value estimated from firn cores (Table 2). An analysis of the averages shows a slight decrease in accumulation since 1998 compared to the 50-year firn core average.

[61] Century-scale variability, computed using Tambora (1816) and atomic bomb marker (1965) accumulation time series from GV7, TD, and 31Dpt, shows a slight increase (of a few percent) in accumulation rates over the last 200 years, in particular, since the 1960s, as compared with the period 1816–1965. Moreover, an analysis across the

period from 1780 to the present shows a flat trend for GV5 and an increase from 3% to 12% for the three other sites.

[62] Snow accumulation time series were smoothed using a 7-year average and stacked to produce a composite record of accumulation rates for the area (Figure 8). The composite curve shows lower values between the beginnings of the series (1800 AD) to 1850 AD. Starting from 1850 AD, near-average accumulation is observed, with an increase occurring from 1960 AD to 1970 AD and during the 1990s. However, stake data show no clear increase in accumulation from 1997 to 2005 AD. Studies in Eastern Wilkes Land and at Dome C [Morgan *et al.*, 1991; Goodwin *et al.*, 2003; Frezzotti *et al.*, 2005] have revealed a pronounced increase in accumulation: +20% and +30%, respectively. These authors attribute the increase in Eastern Wilkes Land to regional air temperature fluctuations and to an increase in cyclonic activity. An analysis of  $\delta D$  at TD [Stenni *et al.*, 2002] shows a slight increase in isotope temperature between 1780 and 1995 AD. To assess the extent of correlation between the snow accumulation time series, different time series (for overlapping 1880–1993 AD period) were normalized with respect to the mean value. No significant correlation was found between the time series from GV7 and the others or between those from GV5 and 31DptA (value lower than 0.20). A moderate negative correlation exists between TD and GV5 ( $R = -0.37$ , at the 99% significance level), and between TD and 31DptA ( $R = -0.48$ , at the 99% significance level) time series. Backward air parcel trajectories, based on the ERA40 reanalysis data set, reveal that 70% of the resulting snowfall trajectories at GV7 come from the Southern Ocean (Indian Sector), whereas at 31Dpt, about 40% come from the Indian Sector and 35% from the Pacific Sector and the Ross Sea. The GV7 core site receives precipitation during synoptic-scale maritime cyclonic incursions coming from the Southern Ocean and shows a frequency from 3 to 7 years, compatible with the Southern Hemisphere Annular Mode. Sites 31DptA and to some extent TD receive maritime cyclonic incursion precipitation from the cooler/dryer Ross Sea area. GV5, TD,

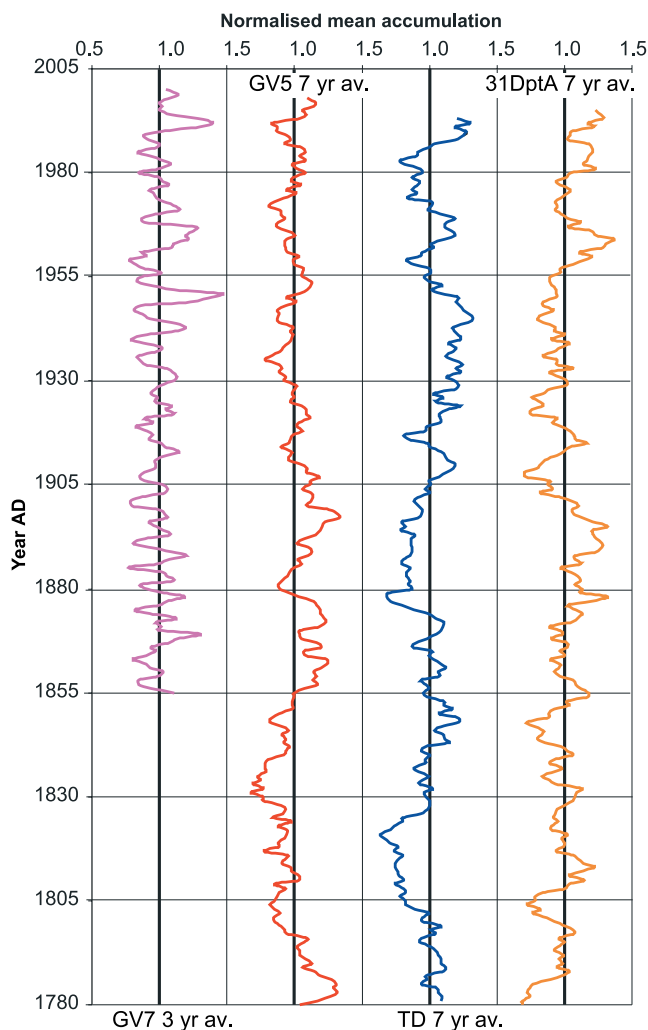


**Figure 8.** Comparison of normalized time series from firn cores of GV7 (3-year average), GV5, TD, and 31DptA (7-year average) that have been normalized with respect to the mean value for the common time period (1855–1996 AD).

and 31DptA core sites are located at higher elevations and receive precipitation from air mass subsidence over the East Antarctic plateau. The TD site is affected by wind-driven sublimation determined by an increase in surface slope toward the Southern Ocean. *Turner et al.* [2005] reported that during the last 50 years, all continental stations have shown a negative trend in mean sea level pressure, and most coastal stations have recorded increasing mean wind speeds over recent decades, because of a change in the Southern Hemisphere Annular Mode. A negative correlation between snow accumulation time series from TD and those from GV5 and 31DptA and a decrease in accumulation at TD over the last 10 years could be linked to postdepositional processes (wind-driven sublimation). Snowfall accumulation across the continent has been investigated by combining mode simulations and observations primarily from firn cores, and the research suggests that there has been no substantial increase but rather a slight downturn in accumulation in the past decade [*Monaghan et al.*, 2006]. Results indicate that there

has been no statistically significant global warming signal of increasing precipitation over Antarctica since the 1950s, from which it may be inferred that the global sea level rise has not been mitigated by recently increased Antarctic snowfall as expected. *Krinner et al.* [2006] pointed out that the link between precipitation and temperature change is more complicated than often assumed. Moreover, an increase in snow precipitation coupled with an increase in temperature and/or wind could result in a decrease in snow accumulation in windy areas [*Frezzotti et al.*, 2004b], such as most of the slope and coastal area in East Antarctica.

## 5. Conclusion

[63] In spite of the fact that the transect is not in a katabatic wind confluence area and does not have an extensive wind crust area, unlike most of the adjacent area of East Antarctica, wind-driven processes are a very important component of snow accumulation at scales ranging from 1 dm to tens of kilometers.

[64] Accumulation records preserved in firn cores are characterized by large interannual variability associated with year-to-year fluctuations in precipitation and the superimposition of meter-scale morphology noise. Detection of “noise,” which largely reflects snow surface roughness (sastrugi), is important since noise limits the degree to which a single annual snow accumulation value observed in a core may be representative of snow accumulation or precipitation on an annual timescale. Frequency analysis of accumulation compared to annual average accumulation shows that data from a single stake (or from a single core) are not representative on an annual scale, even for the site with the highest accumulation. Reconstruction of snow accumulation by core analysis requires very high accumulation values in relation to the level of noise ( $750 \text{ kg m}^{-2} \text{ yr}^{-1}$  for 20- to 40-cm sastrugi height) or a multicore approach if it is to achieve an accuracy comparable to that of instrumental measurements (for example, rain precipitation  $\pm 10\%$ ). Representativeness can be increased by using a multiannual scale with moderate smoothing and improving the accumulation-to-noise ratio. This method can be used to study climate variability on a decadal or secular scale.

[65] Differences between cores and stakes can lead to statistical misidentification of annual layers derived from seasonal signals at sites with accumulation lower than  $200 \text{ kg m}^{-2} \text{ yr}^{-1}$  because of nondetection of higher and lower values ( $\pm 40\%$  compared to the average value). The representativeness of snow chemical and isotopic records is intrinsically related to accumulation values, and the accumulation-to-noise ratio is not a negligible factor in the interpretation of records. The accumulation-to-noise ratio should be taken into account when we seek to interpret seasonal/annual climatic and environmental signals, especially when firn core records are compared or used with atmospheric model and meteorological instrumental records.

[66] The spatial variability of snow accumulation at the kilometer scale (up to  $200 \text{ kg m}^{-2} \text{ yr}^{-1}$  over a 1-km distance) is 1-order-of-magnitude higher than temporal variability at the multidecadal/secular scale. The reconstruction of past climates based on firn/ice cores drilled in areas with spatial variability in snow accumulation is complicated.

[67] Analysis of spatial variability shows that in the coastal area, spatial variability reaches  $200 \text{ kg m}^{-2} \text{ yr}^{-1}$  within the space of 1 km and wind-driven sublimation values may be as high as  $260 \text{ kg m}^{-2} \text{ yr}^{-1}$  (GPR20-GV7). In the plateau area (GV7-31Dpt), spatial variability reaches  $40 \text{ kg m}^{-2} \text{ yr}^{-1}$  within the space of 1 km and wind-driven ablation is as high as  $50 \text{ kg m}^{-2} \text{ yr}^{-1}$ . Redistribution processes are present only on a local scale, with wind-driven sublimation values representing from 20% to 75% of solid precipitation, whereas depositional processes, related to the formation of transverse dunes, are very rare and negligible in the surface mass balance. Wind-driven processes are very important and can sublimate and export huge quantities of snow into the atmosphere and then into the ocean. Wind-driven processes are not negligible in surface mass balance studies.

[68] Wind ablation determined by surface slope along the wind direction is very significant for the purpose of evaluating past, present, and future surface mass balance. It must be taken into account in atmospheric models and when present surface mass balances are compared to precipitation estimated from atmospheric models.

[69] Significant variations in regional annual accumulation have been detected using stake farms. The use of numerical simulation to predict the contribution of Antarctica to sea level rise and remote sensing [Gravity Recovery And Climate Experiment (GRACE), radar-laser altimeter] measurements is significantly hampered by the lack of surface mass balance evaluations and information concerning their variability in space and time. Further studies along these lines will be necessary to determine signal-to-noise variance ratios for surface mass balances and ice core records in other parts of Antarctica.

[70] **Acknowledgments.** Research was carried out in the framework of the Project on Glaciology of the PNRA-MIUR and financially supported by the PNRA Consortium through collaboration with ENEA Roma. This work is a French-Italian contribution to the ITASE. Thanks are due to E. Isaksson, T. Scambos, and N. Inverson whose comments and editing helped to improve the manuscript.

## References

- Arcone, S. A., V. B. Spikes, G. S. Hamilton, and P. A. Mayewski (2004), Stratigraphic continuity in 400-MHz short-pulse radar profiles of firn in West Antarctica, *Ann. Glaciol.*, **39**, 195–200.
- Barnes, P. R. F., E. W. Wolff, and R. Mulvaney (2006), A 44 kyr paleorugness record of the Antarctic surface, *J. Geophys. Res.*, **111**, D03102, doi:10.1029/2005JD006349.
- Becagli, S., et al. (2004), Chemical and isotopic snow variability in East Antarctica along the 2001/02 ITASE traverse, *Ann. Glaciol.*, **39**, 473–482.
- Bintanja, R. (1998), The contribution of snowdrift sublimation to the surface mass balance of Antarctica, *Ann. Glaciol.*, **27**, 251–259.
- Black, H. P., and W. Budd (1964), Accumulation in the region of Wilkes, Wilkes Land, Antarctica, *J. Glaciol.*, **5**(37), 3–15.
- Cullather, R. I., D. H. Bromwich, and M. L. Van Woert (1998), Spatial and temporal variability of Antarctic precipitation from atmospheric methods, *J. Clim.*, **11**, 334–367.
- Déry, S. J., and M. K. Yau (2002), Large-scale mass balance effects of blowing snow and surface sublimation, *J. Geophys. Res.*, **107**(D23), 4679, doi:10.1029/2001JD001251.
- Dibb, J. E., and M. Fahnestock (2004), Snow accumulation, surface height change, and firn densification at Summit, Greenland: Insights from 2 years of in situ observation, *J. Geophys. Res.*, **109**, D24113, doi:10.1029/2003JD004300.
- Eisen, O., U. Nixdorf, F. Wilhelms, and H. Miller (2004), Age estimates of isochronous reflection horizons by combining ice core survey, and synthetic radar data, *J. Geophys. Res.*, **109**, B04106, doi:10.1029/2003JB002858.
- Fischer, H., and D. Wagenbach (1996), Large-scale spatial trends in recent firn chemistry along an east-west transect through central Greenland, *Atmos. Environ.*, **30**, 3227–3238.
- Fisher, D. A., N. Reeh, and H. B. Clausen (1985), Stratigraphic noise in time series derived from ice cores, *Ann. Glaciol.*, **7**, 76–83.
- Folco, L., A. Capra, M. Chiappini, M. Frezzotti, M. Mellini, and I. E. Tabacco (2002), The Frontier Mountain meteorite trap (Antarctica), *Meteorit. Planet. Sci.*, **37**, 209–228.
- Fortuin, J. P. F., and J. Oerlemans (1990), The parameterization of the annual surface temperature and mass balance of Antarctica, *Ann. Glaciol.*, **14**, 78–84.
- Frezzotti, M., and O. Flora (2002), Ice dynamics and climatic surface parameters in East Antarctica from Terra Nova Bay to Talos Dome and Dome C: ITASE Italian Traverses, *Terra Antart.*, **9**(1), 47–54.
- Frezzotti, M., S. Gandolfi, and S. Urbini (2002a), Snow megadune in Antarctica: Sedimentary structure and genesis, *J. Geophys. Res.*, **107**(D18), 4344, doi:10.1029/2001JD000673.
- Frezzotti, M., S. Gandolfi, F. La Marca, and S. Urbini (2002b), Snow dune and glazed surface in Antarctica: New field and remote sensing data, *Ann. Glaciol.*, **34**, 81–88.
- Frezzotti, M., et al. (2004a), Geophysical survey at Talos Dome (East Antarctica): The search for a new deep-drilling site, *Ann. Glaciol.*, **39**, 423–432.
- Frezzotti, M., et al. (2004b), New estimations of precipitation and surface sublimation in East Antarctica from snow accumulation measurements, *Clim. Dyn.*, **23**(7–8), doi:10.1007/s00382-004-0462-5.
- Frezzotti, M., et al. (2005), Spatial and temporal variability of snow accumulation in East Antarctica from traverse data, *J. Glaciol.*, **51**(207), 113–124.
- Gallée, H. (1998), Simulation of blowing snow over the Antarctic ice sheet, *Ann. Glaciol.*, **26**, 203–206.
- Gallée, H., G. Guyomarch, and E. Brun (2001), Impact of snow drift on the Antarctic Ice Sheet surface mass balance: Possible sensitivity to snow-surface properties, *Boundary Layer Meteorol.*, **99**, 1–19.
- Gallée, H., V. Peyaud, and I. Goodwin (2005), Simulation of the net snow accumulation along the Wilkes Land transect, Antarctica, with a regional climate model, *Ann. Glaciol.*, **41**, 17–22.
- Gandolfi, S., M. Milano, and L. Gusella (2005), Precise Point Positioning: Studio sulle accuratezze e precisioni ottenibili, ed applicabilità dell'approccio, *Boll. Geod. Sci. Affini*, **4**, 227–253.
- Genthon, C., and G. Krinner (2001), The Antarctic surface mass balance and systematic biases in GCMs, *J. Geophys. Res.*, **106**, 20,653–20,664.
- Giovinetto, M. B., N. M. Waters, and C. R. Bentley (1990), Dependence of Antarctic surface mass balance on temperature, elevation, and distance to open ocean, *J. Geophys. Res.*, **95**(D4), 3517–3531.
- Goodwin, I. D. (1991), Snow-accumulation variability from seasonal surface observations and firn-core stratigraphy, eastern Wilkes Land, Antarctica, *J. Glaciol.*, **37**(127), 383–387.
- Goodwin, I. D., H. De Angelis, M. Pook, and N. W. Young (2003), Snow accumulation variability in Wilkes Land, East Antarctica and the relationship to atmospheric ridging in the  $130^{\circ}$ – $170^{\circ}$ E region since 1930, *J. Geophys. Res.*, **108**(D21), 4673, doi:10.1029/2002JD002995.
- Gow, A. J. (1965), On the accumulation and seasonal stratification of snow at the South Pole, *J. Glaciol.*, **5**, 467–477.
- ISMALSS Committee (2004), Recommendations for the collection and synthesis of Antarctic Ice Sheet mass balance data, *Global Planet. Change*, **42**(1–4), 1–15.
- Krinner, G., O. Magand, I. Simmonds, G. Genthon, and J. L. Dufresne (2006), Simulated Antarctic precipitation and surface mass balance at the end of the twentieth and twenty-first centuries, *Clim. Dyn.*, doi:10.1007/s00382-006-0177-x2006.
- Lorius, C. (1983), Accumulation rate measurements on cold polar glaciers, in *The Climatic Record in Polar Ice Sheets*, edited by G. Q. de Robin, pp. 65–70, Cambridge Univ. Press, New York.
- Magand, O., M. Frezzotti, M. Pourchet, B. Stenni, L. Genoni, and M. Fily (2004), Climate variability along latitudinal and longitudinal transects in East Antarctica, *Ann. Glaciol.*, **39**, 351–358.
- Mancini, M., and M. Frezzotti (2003), Surface wind field along IT-ITASE traverse (East Antarctica), *Terra Antart. Rep.*, **8**, 57–59.
- Mayewski, P. A., and I. D. Goodwin (1999), Antarctic's role pursued in global climate change, *Eos Trans. AGU*, **80**, 398–400.
- McConnell, J. R., R. C. Bales, and D. R. Davis (1997), Recent intra-annual snow accumulation at South Pole: Implications for ice core interpretation, *J. Geophys. Res.*, **102**(D18), 21,947–21,954.
- Monaghan, A. J., et al. (2006), Insignificant change in Antarctic snowfall since the international geophysical year, *Science*, **313**, 827–831.
- Morgan, V., I. Goodwin, D. Etheridge, and C. Wookey (1991), Evidence from Antarctic ice cores for recent increases in snow accumulation, *Nature*, **354**, 58–60.

- Mosley-Thompson, E., L. G. Thompson, J. F. Paskievitch, M. Pourchet, A. J. Gow, M. E. Davis, and J. Kleinman (1995), Recent increase in South Pole snow accumulation, *Ann. Glaciol.*, *21*, 131–138.
- Muszynski, I., and G. E. Birchfield (1985), The dependence of Antarctic accumulation rates on surface temperature and elevation, *Tellus*, *37A*, 204–208.
- Negusini, M., F. Mancini, S. Gandolfi, and A. Capra (2005), Terra Nova Bay GPS permanent station (Antarctica): data quality and first attempt in the evaluation of regional displacement, *J. Geodyn.*, *39*, 81–90.
- Neilan, R. E. J. F. Zumberge G. Beutler and J. Kouba (1997), The International GPS Service: A Global Resource for GPS Applications and Research. Proceedings of the ION GPS-97, Kansas City, Missouri.
- Noone, D., J. Turner, and R. Mulvaney (1999), Atmospheric signals and characteristics of accumulation in Dronning Maud Land, Antarctica, *J. Geophys. Res.*, *104*(D16), 19,191–19,211.
- Paillard, D., L. Labeyrie, and P. Yiou (1996), Macintosh program performs time-series analysis, *Eos Trans. AGU*, *77*, 379.
- Palais, J. M., I. M. Whillans, and C. Bull (1982), Snow stratigraphic studies at Dome C, East Antarctica: An investigation of depositional and diagenetic processes, *Ann. Glaciol.*, *3*, 239–242.
- Paris, T. R., and D. H. Bromwich (1991), Continental scale of the Antarctic katabatic wind regime, *J. Clim.*, *4*(2), 135–146.
- Petit, J. R., J. Jouzel, M. Pourchet, and L. Merlivat (1982), A detailed study of snow accumulation and stable isotope content in Dome C (Antarctica), *J. Geophys. Res.*, *87*(C6), 4301–4308.
- Rémy, F., P. Shaeffer, and B. Legresy (1999), Ice flow physical processes derived from ERS-1 high-resolution map of the Antarctica and Greenland ice sheet, *Geophys. J. Int.*, *139*, 645–656.
- Richardson, C., E. Aarholt, S.-E. Hamran, P. Holmlund, and E. Isaksson (1997), Spatial distribution of snow in western Dronning Maud Land, East Antarctica, mapped by a ground-based snow radar, *J. Geophys. Res.*, *102*(B9), 20,343–20,354.
- Spikes, V. B., S. Arcone, G. Hamilton, P. Mayewski, D. Dixon, and S. Kaspari (2004), Spatial and temporal variability in West Antarctic snow accumulation rates, *Ann. Glaciol.*, *39*, 238–244.
- Stearns, C. R. and G. A. Weidner (1993), Sensible and Latent Heat Flux Estimates in Antarctic, in *Antarctic Meteorology and Climatology: Studies Based on Automatic Weather Stations*, Antarctic Res. Ser., vol. 61, edited by D. H. Bromwich and C. R. Stearns pp. 109–138, AGU, Washington, D. C.
- Stenni, B., M. Proposito, R. Gragnani, O. Flora, J. Jouzel, S. Falourd, and M. Frezzotti (2002), Eight centuries of volcanic signal and climate change at Talos Dome (East Antarctica), *J. Geophys. Res.*, *107*(D9), 4076, doi:10.1029/2000JD000317.
- Turner, J., S. R. Colwell, G. J. Marshall, T. A. Lachlan-Cope, A. M. Carleton, P. D. Jones, V. Lagun, P. A. Reid, and S. Lagovkina (2005), Antarctic climate change during the last 50 years, *Int. J. Climatol.*, *25*, 279–294.
- van den Broeke, M. R. (1997), Spatial and temporal variation of sublimation on Antarctica: Results of a high-resolution general circulation model, *J. Geophys. Res.*, *102*(D25), 29,765–29,778, doi:10.1029/97JD01862.
- van den Broeke, M. R., C. H. Reijmer, and R. S. W. van de Wal (2004), A study of the surface mass balance in Dronning Maud Land, Antarctica, using automatic weather stations, *J. Glaciol.*, *50*(171), 565–582.
- van der Veen, C. J., E. Mosley-Thompson, A. J. Gow, and B. G. Mark (1999a), Accumulation at South Pole: Comparison of two 900-year records, *J. Geophys. Res.*, *104*(D24), 31,067–31,076.
- van der Veen, C. J., I. M. Whillans, and A. J. Gow (1999b), On the frequency distribution of net annual snow accumulation at the South Pole, *Geophys. Res. Lett.*, *26*(2), 239–242.
- Vaughan, D. G., H. J. F. Corr, C. S. M. Doake, and E. D. Waddington (1999), Distortion of isochronous layers in ice revealed by ground-penetrating radar, *Nature*, *398*(6725), 323–326.
- Vittuari, L., C. Vincent, M. Frezzotti, F. Mancini, S. Gandolfi, G. Bitelli, and A. Capra (2004), Space geodesy as a tool for measuring ice surface velocity in the Dome C region and along the ITASE traverse, *Ann. Glaciol.*, *39*, 402–408.
- Zumberge, J. F., M. B. Helfin, D. C. Jefferson, M. M. Watkins, and F. H. Webb (1997), Precise point positioning for the efficient and robust analysis of GPS data from large networks, *J. Geophys. Res.*, *102*(B3), 5005–5018.

M. Frezzotti, M. Proposito, and C. Scarchilli, Ente per le Nuove Tecnologie, l'Energia e l'Ambiente, Rome, Italy.

S. Gandolfi, Dipartimento di Ingegneria delle Strutture, dei Trasporti, delle Acque, del Rilevamento, del Territorio, University of Bologna, Bologna, Italy.

C. Scarchilli, Dipartimento di Scienze della Terra, University of Siena, Siena, Italy.

S. Urbini, Istituto Nazionale di Geofisica e Vulcanologia, Rome, Italy.